The CELESTA CubeSat In-Flight Radiation Measurements and Their Comparison With Ground Facilities Predictions

Andrea Coronetti, *Associate Member, IEEE*, Alessandro Zimmaro, Rubén García Alía, *Member, IEEE*, Salvatore Danzeca, Alessandro Masi, Ivan Slipukhin, Alessio Amodio, Jasper Dijks, Paul Peronnard, Raffaello Secondo, Markus Brugger, Enrico Chesta, Muriel Bernard, Laurent Dusseau, Tristan Allain, Rafael Mendes Duarte, Jean-Roch Vaillé, Frédéric Saigné, Jerome Boch, and Luigi Dilillo, *Member, IEEE*

***Abstract*— The CELESTA CubeSat has employed radiation monitors developed by the Conseil Européen pour la Recherche Nucléaire (CERN) Centre, used for measuring the radiation environment at accelerators, to measure the space radiation field in a medium-Earth orbit (MEO). The technology is based on three static random-access memories (SRAMs) that are sensitive to single-event upsets (SEUs) and single-event latchups (SELs). The measurements were performed for the duration of two months. A statistically significant amount of SEUs and SELs was collected. No solar proton event effects were observed in the data during this period. The in-flight rates were compared with respect to estimations coming from the environmental space fluxes available in the Outil de Modelisation de l'Environmment Radiative Externe (OMERE) tool suite and ground facility measurements done with ions and protons. The analysis emphasizes the importance of employing more sophisticated satellite shielding models for the calculation of the fluxes reaching the detectors as well as the need to know accurately the proton energy threshold of the SEU cross section Weibull response of the devices. Both observations mainly arise from the peculiar spectral distribution of protons in this MEO peaking at 10–20 MeV, which differs from those of a low-Earth orbit (LEO) environment.**

***Index Terms*— CERN Highly AcceleRated Mixed-field (CHARM), commercial devices, CubeSat, in-flight measurements, radiation monitor, SEE.**

Manuscript received 22 February 2024; revised 10 March 2024; accepted 10 March 2024. Date of publication 13 March 2024; date of current version 16 August 2024. This work was supported in part by the European Organization for Nuclear Research (CERN) Knowledge Transfer Fund and Radiation to Electronics (R2E) Project through the CERN Latchup and Radmon Experiment Student Satellite (CELESTA) CubeSat Project, in part by the European Space Agency (ESA) for the Vega-C Launch, and in part by the Fondation Van Allen (FVA). *(Corresponding author: Andrea Coronetti.)*

Andrea Coronetti, Alessandro Zimmaro, and Ivan Slipukhin are with CERN, CH-1211 Geneva, Switzerland, and also with the Institute d'Électronique et des Systèmes, Université de Montpellier, 34090 Montpellier, France (e-mail: andrea.coronetti@cern.ch).

Rubén García Alía, Salvatore Danzeca, Alessandro Masi, Alessio Amodio, Jasper Dijks, Paul Peronnard, Raffaello Secondo, Markus Brugger, and Enrico Chesta are with CERN, CH-1211 Geneva, Switzerland.

Muriel Bernard, Laurent Dusseau, Tristan Allain, and Rafael Mendes Duarte are with the Center Spatial Universitaire de Montpellier, Institute d'Électronique et des Systèmes, Université de Montpellier, 34090 Montpellier, France.

Jean-Roch Vaillé, Frédéric Saigné, and Jerome Boch are with the Institute d'Électronique et des Systèmes, Université de Montpellier, 34090 Montpellier, France.

Luigi Dilillo is with the Institute d'Électronique et des Systémes, Université de Montpellier, CNRS, 34090 Montpellier, France.

Color versions of one or more figures in this article are available at https://doi.org/10.1109/TNS.2024.3376749.

Digital Object Identifier 10.1109/TNS.2024.3376749

I. Introduction

SPACE radiation environment characterization is a key aspect for ensuring proper radiation hardness assurance to all space missions employing electronic devices and operating in orbits around the Earth and in deep space. Similarly, developing ground-level radiation facilities that can provide environmental conditions capable of mimicking the effects of radiation in space is also instrumental in ensuring that proper radiation hardness assurance can be achieved.

Over the last two decades, several efforts have been made toward creating standardized modular radiation monitors that can be easily adapted to many different satellites. Many of these monitors are based on sophisticated radiation monitors that can detect different kinds of particles and resolve their energy [1], [2]. Others are based on low-cost detectors, e.g., static random-access memories (SRAMs) that can characterize the radiation environment by measuring single-event upsets (SEU) or single-event latchups (SELs) [3], [4], [5], [6], [7], [8], [9], [10], [11], [12], [13], [14], [15], [16], [17]. Often these radiation monitors can also be used to characterize beams at facilities. Several calculation methods [18], [19], [20], [21] are available to verify the expected space sensitivity of these monitors. They can also be used to verify the suitability of such prediction methods.

The Conseil Européen pour la Recherche Nucléaire (CERN) has been developing similar radiation monitoring systems for the Large Hadron Collider (LHC) [22]. These have total ionizing dose (TID) monitoring capabilities through the use of RADFETs and fluence measurement capabilities thanks to the assessment of SEUs and their rate. The radiation monitoring system on-board the CELESTA CubeSats builds on these capabilities and partly expands them by embedding an additional SEL experiment for fluence cross-comparison measurements.

The CELESTA CubeSat and its radiation monitoring system is based on the Centre Spatial de l'Université de Montpellier (CSUM) 1U v3.5 in-house CubeSat platform. It has undergone a four-year development directed by CSUM and CERN [23]. The work included the development of the flat-sat model, the engineering model, the proto-flight model, and the radiation model. The qualification included full functional testing, thermal vacuum testing, and vibration testing in

accordance with the Vega-C interface control document. Concerning radiation, this process included the calibration of radiation monitors, such as the SRAMs [24], [25] and the full system-level qualification of the CubeSat at the CERN Highly AcceleRated Mixed-field (CHARM) facility [26], [27]. After passing the calibration and qualification stages, the CELESTA CubeSat was launched on July 13, 2022, by a VEGA-C launcher during its maiden flight. The CubeSat collected data for the two months that followed, until it reached the end of mission on September 12, 2022.

In this article, a summary of the in-flight data measurements for the payload of the CubeSat is reported. The data are then compared with rate predictions for the operational orbit that were determined following the detector calibration in ground-level facilities delivering ions and protons and mixed-field radiation.

II. Payload Description and Mission Profile

The radiation monitor on-board the CELESTA CubeSat is a single board that embeds a radiation field effect transistor (RADFET) for TID measurement, a Cypress SRAM for SEU measurements, and two Brilliance SRAMs for SEL measurements. This board can be seen in Fig. 1. In the final configuration, the board is mounted on top of three other printed circuit boards (PCBs), of the battery casing, and of the battery itself. A cartoon of this configuration is presented in Fig. 2. From the front side, the detectors are facing the outer space with just the solar panel and the external wall shielding in the way. This enables minimal shielding with respect to the space particles coming from the front side hemisphere, i.e., about 2.1 mm of equivalent aluminum. However, the shielding effect on the back side is much stronger due to the rest of the material composing the CubeSat.

Concerning the commercial SRAMs, the Cypress SRAM is a CY62157EV30LL-45ZSXI, a 90 nm technology with 8 Mbit storage capacity and lot date code 1037. During the flight, it was biased at the nominal 3.3 V and written with a checkerboard pattern. The Brilliance SRAM is a BS62LV1600EIP55, a 180 nm technology with 16 Mbit storage capacity and lot date code 12094. Due to the very high SEL sensitivity of the device only the SEL experiment was performed on this SRAM, and no SEU measurements were taken.

A ProASIC3 field programmable gate array (FPGA) performs the SEU readout of the Cypress SRAM and the current monitoring for the Brilliance SRAM. For each Brilliance SRAM, the FPGA controls a conditioning circuit, consisting of several stages, designed to detect SELs on memories. First, a difference amplifier measures the voltage difference between the 5 V reference provided by the on-board computer (OBC) and the input voltage of the dc–dc converter supplying the SRAM. To reduce the impact of the voltage drop over the input resistor on the component biasing and latch-up sensitivity, a low-resistance value is used. The output of the difference amplifier is then compared with a reference voltage of 1.2 V using an operational amplifier in a voltage comparator configuration. Finally, the output is read by the FPGA for SEL detection. When the comparator output is high, the FPGA checks its stability for 5 ms. In case it reaches this threshold,

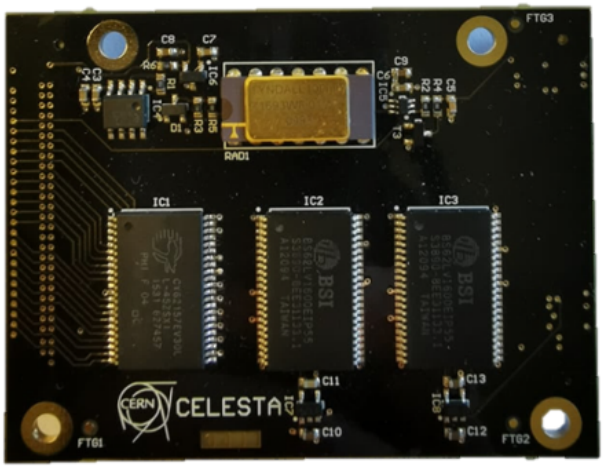

Fig. 1. Radiation monitoring system board of the CELESTA CubeSat [25].

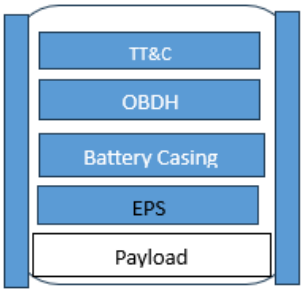

Fig. 2. Cartoon of the CELESTA CubeSat PCB stack-up, including the telemetry, tracking, and control (TT&C), on-board data handling (OBDH), electric power system (EPS), the battery, and the payload.

the FPGA deactivates the dc–dc converter for 50 ms, which power cycles the Brilliance SRAM and clears the SEL. At the same time, a counter is increased to keep track of the number of SEL events. On the other hand, if the above condition is not met, the event is not counted as an SEL.

For the Cypress SRAM and the analog–digital converter (ADC), used to read the RADFET, the FPGA design implements a finite state machine (FSM) used to disable, enable, and time the different operations related to these sensors and the payload data transmission. The FSM starts in an idle state by default to keep the SRAM and ADC in power-safe mode, thus reducing power consumption of the payload. When the satellite is set in commissioning mode, the FSM state is changed and the SRAM and RADFET are read, respectively, every 240 and 110 s. Finally, when in data transmission mode, the FSM also controls the controlled area network (CAN) transmission, activating it every 120 s and allowing CELESTA to transmit raw data to the OBC. All this information is also presented graphically in previous CELESTA-related publications [25], [26].

The data were collected by the OBC and stored in its internal memory until transmission with the ground station was available. The data stored in the OBC were under the form of an incremental counter for the SEU and SEL measurements. Therefore, no timestamps regarding the occurrence of the events were recorded, and no geolocalization of the SEUs and SELs is possible. The only timestamp tagged to the data

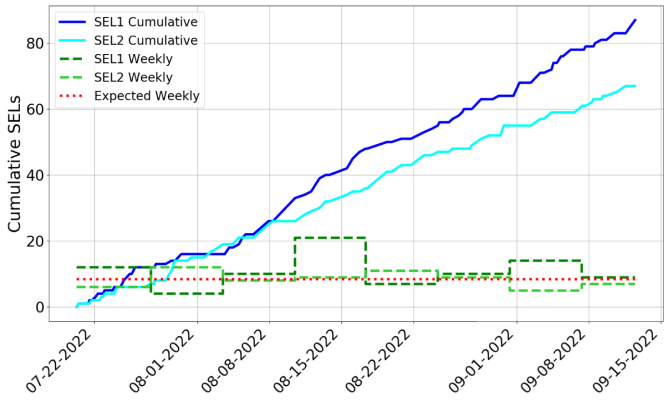

Fig. 3. In-flight SEL measurements as a function of time for the two Brilliance SRAMs for the whole mission duration, cumulative, and weekly data. Expected weekly data are based on calculations in Table III for proton measurements with Weibull fit with mixed-shielding.

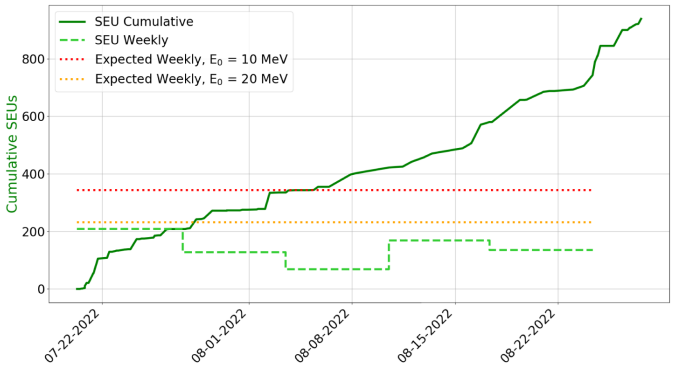

Fig. 4. In-flight SEU measurements as a function of time for the Cypress SRAM before the failure, cumulative, and weekly data. Expected weekly data are based on calculations in Table IV for proton measurements with Weibull fit with mixed-shielding.

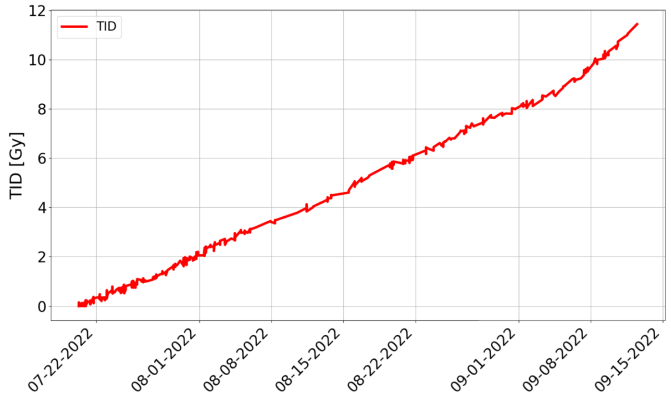

Fig. 5. In-flight TID measurements as a function of time for the whole mission duration.

is that of the time at which the transmission to the ground station occurred. The criticality of collecting such data is well understood, and efforts will be devoted to ensure that future missions, already set, will include the SEE geolocalization capability.

The CubeSat operated in a quasi-circular medium-Earth orbit (MEO) whose orbital parameters are as follows.

1) Perigee altitude: 5865.4 km
2) Apogee altitude: 5866.9 km
3) Inclination: 70.16°
4) Right ascension of the ascending node (RAAN): −52.3°
5) Argument of perigee: 142.9°
6) Orbital period: 3.74 h

The CubeSat was fully commissioned and fully operational on July 20, 2022, when the first data from the radiation monitoring system were received. The data logging received from the satellite has not been fully regular due to the limited availability of the ground station, but no data were lost.

III. Flight Measurements Summary

Fig. 3 presents the cumulative in-flight SELs as a function of mission time from the first data reception up to the definitive loss of communication with the satellite. The cumulative data for the two SRAMs are presented separately. Less than 100 SELs on each SRAM were recorded during the mission timeline, but, overall, the two SRAMs showed good agreement with one another. The measured SEL flight rate in this orbit was 1.59 SEL/day for SRAM 1 and 1.22 SEL/day for SRAM 2. The figure also shows the data broken down on a week-by-week basis for the two SRAMs and that these data are aligned with the predicted SEL rate that is calculated later.

Fig. 4 presents the cumulative in-flight SEUs as a function of mission time from the first data reception. This experiment was no longer functional after August 27, 2022, due to an issue with the FPGA counter. Up to that point, the time progression of the cumulative SEUs was still linear and more than 800 SEUs were accumulated. This results in an in-flight SEU rate of 17 SEU/day. Also, here the per week data are presented and compared with a couple of predictions calculated later. It is worth mentioning that the Cypress also experienced multiple bit upsets (MBUs) in a ratio of 1 MBU every 20 single bit upsets (SBUs).

Fig. 5 displays the cumulative in-flight TID as a function of the mission time from the first data reception up to the end of the mission. A rather linear progression can be identified with a slight change of slope toward the end of the mission. Overall, the RADFET saw less than 12 Gy(Si) [or 1.2 krad(Si)] for the whole mission.

Fig. 6 shows that the progression in terms of accumulation of SEUs in the Cypress, of SELs in the Brilliance, and of TID followed a very similar linear trend for the period in which the data for the Cypress SRAM were correctly logged.

IV. Ground Facilities and Rate Predictions

A. Experimental Data Collection at Facilities

Several SRAMs were considered as possible candidates for the CELESTA radiation monitoring system during the development phase of this project. As a result, the data collection in terms of SEU and SEL cross sections at ground facilities was spread out in time. In some cases, SEU and SEL cross sections for the exact flight lots were not collected, but they were collected on different lots of the same SRAMs.

Concerning the SEL measurements for the Brilliance SRAM, heavy ion SEL cross sections on the flight lot were collected at the Université Catholique de Leuven (UCL) by the

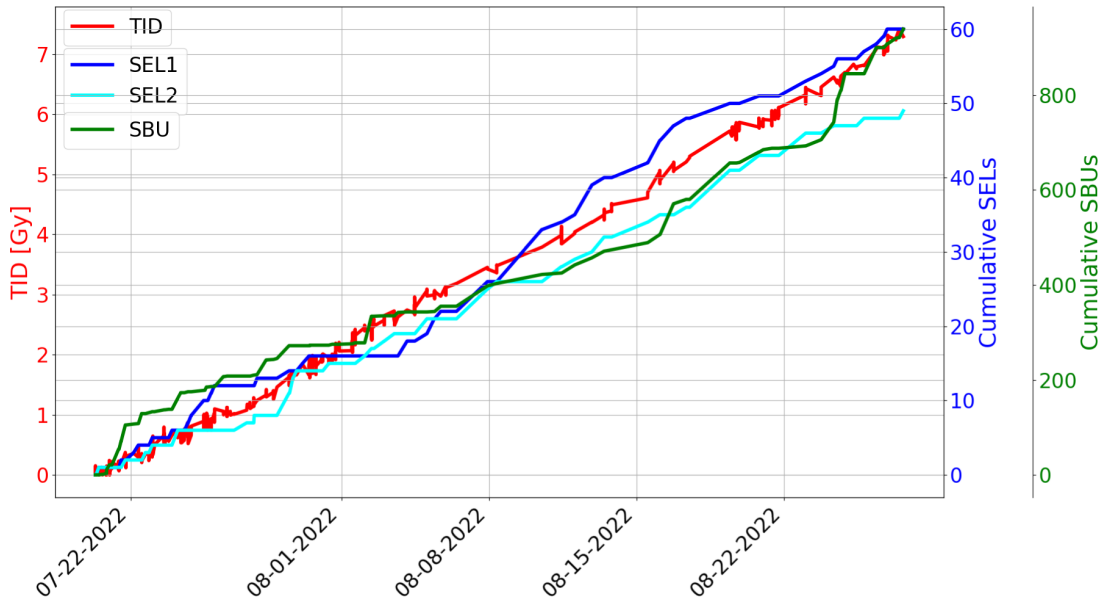

Fig. 6. In-flight TID, SEL, and SEU measurements as a function of time until August 27, 2022.

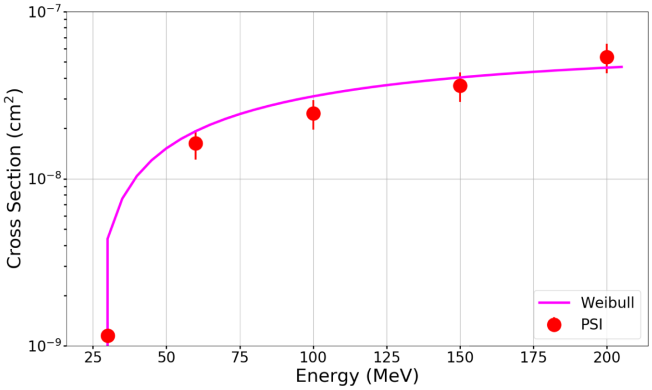

Fig. 7. Proton SEL cross section measurements at PSI and Weibull fit for the Brilliance SRAM.

TABLE I

WEIBULL PARAMETERS FOR ION SEU CROSS SECTION MEASUREMENTS ON THE CYPRESS SRAM [28] AND SEL CROSS SECTION MEASUREMENTS ON THE BRILLIANCE SRAM [29]. FOR THE CYPRESS, THE CROSS SECTION IS PER BIT

SRAM	σ_{sat} [cm^2]	LET$_0$ [MeV/(mg/cm^2)]	W [MeV/(mg/cm^2)]	s
Cypress	1.6×10^{-7}	0.1	30	1.8
Brilliance	5×10^{-2}	2.9	3.79	1.9

TABLE II

WEIBULL PARAMETERS FOR PROTON SEU CROSS SECTION MEASUREMENTS ON THE CYPRESS SRAM [28] AND SEL CROSS SECTION MEASUREMENTS ON THE BRILLIANCE SRAM. FOR THE CYPRESS, THE CROSS SECTION IS PER BIT

SRAM	σ_{sat} [cm^2]	E$_0$ [MeV]	W [MeV]	s
Cypress	8.9×10^{-14}	10-20	21-17	1.2-1.5
Brilliance	5.9×10^{-8}	25	105.8	0.84

European Space Agency (ESA) [3]. The high-energy proton (HEP) data for the flight lot were collected at the Paul Scherrer Institute (PSI) by CERN. These proton data were collected in 2014, but were not published before. They are displayed in Fig. 7 along with the Weibull fit. 95% confidence level error bars are added to the experimental points and are based on the 10% uncertainty on the fluence. Finally, some measurements were also performed at the CHARM mixed-field facility on the flight lot by CERN [23], [26].

For the SEU measurements on the Cypress SRAM, heavy ion and proton SEU data on different lots than the flight lots were collected at the University Medical Center of Groningen (UMCG) and at the Grand Accélerateur National de Ions Lourdes (GANIL) by CERN [28]. Measurements were also performed at the CHARM mixed-field facility on the flight lot by CERN [23].

Table I reports the ion Weibull parameter data for the Cypress and Brilliance SRAMs that were collected from previously published works. Table II gives the proton Weibull parameter data for the Cypress and Brilliance SRAMs that were collected from previous published works or whose fit is provided in this work. For the Cypress SRAM, the proton data collected did not allow for establishing an energy threshold for the Weibull curve. The lowest energy data point was collected at 40 MeV, and the cross section was still close to saturation. Therefore, it can be assumed that the energy threshold for this memory is below 20 MeV and likely above 10 MeV. Both extreme values will be retained for the calculations later on. Slightly different Weibull shape and exponent parameters are used for the two energy thresholds and are indicated in the table. The two Weibull functions and the experimental data points are reported in Fig. 8. 95% confidence level error bars are plotted for the experimental data and were calculated assuming 10% uncertainty on the fluence.

In addition to these data, CHARM cross sections are also reported. It is worth recalling that, for the CHARM test,

TABLE III

BRILLIANCE SEL RATE PREDICTIONS FROM OMERE FOR HEAVY ION, HEP, AND CHARM DATA COMPARED TO THE FLIGHT RATES. SPACE FLUXES WERE TRANSPORTED THROUGH 2.1 mm OF ALUMINUM OR THROUGH THE MORE REALISTIC MIXED-SHIELDING CONFIGURATION. THE WEIBULL [18] AND STEP [30] CALCULATION METHODS ARE REPORTED

Rate type	Experimental data	Method	Shielding	Rate [SEL/day]
Heavy ion	UCL	Weibull	2.1 mm Al	0.29
Heavy ion	UCL	Weibull	Half 2.1 mm + half 20 mm Al	0.25
Proton	PSI	Weibull	2.1 mm Al	1.33
Proton	PSI	Weibull	Half 2.1 mm + half 20 mm Al	0.87
Proton	CHARM	Step	2.1 mm Al	1.86
Proton	CHARM	Step	Half 2.1 mm + half 20 mm Al	1.05
All particles	UCL + PSI	Weibull	2.1 mm Al	1.62
All particles	UCL + PSI	Weibull	Half 2.1 mm + half 20 mm Al	1.12
All particles	UCL + CHARM	Step	2.1 mm Al	2.15
All particles	UCL + CHARM	Step	Half 2.1 mm + half 20 mm Al	1.30
In-flight SEL1				1.59
In-flight SEL2				1.22

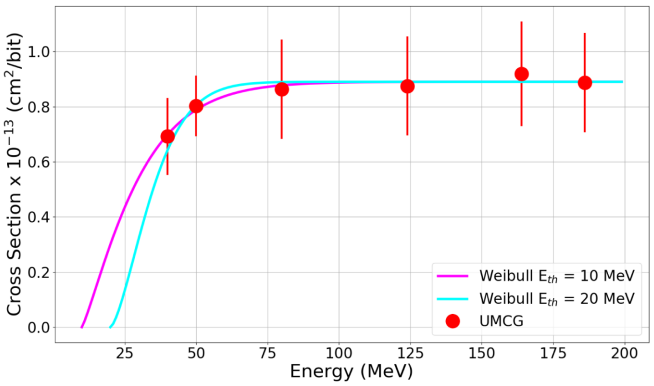

Fig. 8. Proton SEU cross section Weibull fits for the Cypress SRAM measured at UMCG.

a single high-energy hadron equivalent (HEH_{eq}) cross section is reported. Its meaning was previously presented [30], but, in short, this is the cross section obtained by using the integral high-energy hadron (protons, neutrons, pions, and other hadrons) fluence above 20 MeV plus a weighted contribution from neutrons below 20 MeV, in the SEU case. For the Cypress SRAM, the measured SEU cross section at CHARM was 1.65×10^{-13} cm^2/bit, which is almost a factor of two higher than the saturation cross section measured at PSI. For the Brilliance SRAM the measured SEL cross section at CHARM was 1.33×10^{-8} cm^2, which is about a factor of five lower than the proton saturation cross section measured at PSI.

B. Rate Prediction Methods and Parameters

The environment for this orbit during the two month mission period was simulated by means of the Outil de Modelisation de l'Environnement Radiative Externe (OMERE) version 5.2.5 tool suite [31]. The AP8min model [32] was used in combination with the Jensen-Cain geomagnetic field model to derive the trapped proton fluxes in the 100 keV–300 MeV range. The galactic cosmic ray (GCR) fluxes for all ions up to Uranium were calculated through the GCR ISO 15390:2004 model [33] with the Störmer geomagnetic cutoff.

Concerning solar particle events, a posteriori, the only relevant solar event during the mission duration occurred on August 28. No significant jump in the cumulative SELs at this time was noticed for the two Brilliance SRAMs. Concerning the Cypress SRAM, the reliable data acquisition window stops just before this event. In conclusion, no data from solar particle events that can be used for comparison to a prediction method are available.

An initial prediction is performed by taking the fluxes arising from these various sources and transporting them through the 2.1 mm aluminum spherical isotropic shielding. This can be assumed to be a rather accurate estimation of the shielding only for the 2π sr solid angle standing on the payload board side on which the SRAMs are mounted. For the other side, the shielding given by the rest of the satellite components is much higher and, on average, it can be assumed to reach 20 mm of equivalent aluminum. A first calculation was performed considering the 2.1 mm to apply to the whole 4π sr solid angle. A second calculation took into account the increased shielding on the bottom hemisphere.

The OMERE tool suite was used to calculate the rates from the determined particle fluxes by means of the cross sections measured experimentally at the various facilities. For the ion contribution, the ion fluxes were convolved with the Weibull function. The cell depth is an important parameter for the ion response and was set at 0.5 μm for the Cypress SRAM SEU rate calculations. This dimension is based on an extrapolation with respect to Monte-Carlo (MC) rectangular parallelepiped models on 65-nm SRAMs from Cypress. For the Brilliance SRAM SEL rate calculations, this was set to 2 μm in accordance with previous MC simulations for this technology [34]. The same approach can be followed to determine the proton SEU rate by means of the Weibull curve, although in this case, the sensitive volume thickness has less importance. For the CHARM data, since only one cross section is available, the calculation method is again done in OMERE by inputting only the HEH_{eq} cross section as the saturation cross section and 20 MeV as the threshold energy. This corresponds to applying a step response function to the proton fluxes starting at 20 MeV.

Table III presents the calculated SEL rates for the Brilliance SRAM based on the cross sections measured at ground facilities. The information is detailed to show the contributions from

TABLE IV

CYPRESS SEU RATE PREDICTIONS FROM OMERE FOR HEAVY ION, HEP, AND CHARM DATA COMPARED TO THE FLIGHT RATES. SPACE FLUXES WERE TRANSPORTED THROUGH 2.1 mm OF ALUMINUM OR THROUGH THE MORE REALISTIC MIXED-SHIELDING CONFIGURATION. ENERGY THRESHOLD USED FOR THE HEP WEIBULL CURVE WAS 10 OR 20 MeV. THE BENDEL [35] METHOD IS ALSO REPORTED WITH BENDEL PARAMETERS $E_0 = 4$ MeV, $\sigma_{SAT} = 1.2 \times 10^{-13}$ cm^2/Bit, A = 4, B = 3.439. THE WEIBULL, STEP, AND FOM [36] CALCULATION METHODS ARE ALSO REPORTED

Rate type	Experimental data	Method	Shielding	Rate [SEL/day]
Heavy ion	UMCG-GANIL	Weibull	2.1 mm Al	1.78
Heavy ion	UMCG-GANIL	Weibull	Half 2.1 mm + half 20 mm Al	1.52
Proton	UMCG	Weibull E_0 = 10 MeV	2.1 mm Al	84.46
Proton	UMCG	Weibull E_0 = 10 MeV	Half 2.1 mm + half 20 mm Al	48.38
Proton	UMCG	Weibull E_0 = 20 MeV	2.1 mm Al	52.35
Proton	UMCG	Weibull E_0 = 20 MeV	Half 2.1 mm + half 20 mm Al	31.90
Proton	UMCG	Bendel	2.1 mm Al	69.65
Proton	UMCG	Bendel	Half 2.1 mm + half 20 mm Al	40.32
Proton	UMCG	FOM	2.1 mm Al	20.16
Proton	UMCG	FOM	Half 2.1 mm + half 20 mm Al	12.09
Proton	CHARM	Step	2.1 mm Al	194.47
Proton	CHARM	Step	Half 2.1 mm + half 20 mm Al	109.95
All particles	UMCG-GANIL	Weibull E_0 = 10 MeV	2.1 mm Al	85.56
All particles	UMCG-GANIL	Weibull E_0 = 10 MeV	Half 2.1 mm + half 20 mm Al	49.27
All particles	UMCG-GANIL	Weibull E_0 = 20 MeV	2.1 mm Al	53.27
All particles	UMCG-GANIL	Weibull E_0 = 20 MeV	Half 2.1 mm + half 20 mm Al	32.72
All particles	UMCG-GANIL	Bendel	2.1 mm Al	71.47
All particles	UMCG-GANIL	Bendel	Half 2.1 mm + half 20 mm Al	41.90
All particles	UMCG-GANIL	FOM	2.1 mm Al	21.94
All particles	UMCG-GANIL	FOM	Half 2.1 mm + half 20 mm Al	13.86
All particles	UMCG-GANIL + CHARM	Step	2.1 mm Al	195.45
All particles	UMCG-GANIL + CHARM	Step	Half 2.1 mm + half 20 mm Al	111.11
In-flight SEU				17

ions and protons according to OMERE. Then, the table reports the overall rate from all particles and the flight rates for the two SRAMs. For the proton rate predictions, both the calculated rates from HEP and those from CHARM are reported.

For simplicity, proton data from various sources are merged together. Nevertheless, the contribution of solar and GCR protons for this orbit is two orders of magnitude lower than those from trapped protons. Therefore, one can take the total proton rate as fully coming from trapped protons. The GCR ions contribute only a very small percentage on the total rate (<5%). The overall SEL rate is therefore dominated by the trapped protons, for both the PSI and CHARM-based estimates. Both predicted rates are very close to one another. The PSI prediction fits well the flight rate. The CHARM prediction can also be considered to be fitting well to the flight rates, within less than a factor of two difference.

Table IV presents the calculated SEU rates for the Cypress SRAM based on the cross sections measured at ground facilities. Most of the aforementioned considerations for the SEL case still apply to the SEU data, and dominance from trapped protons is still present in the predicted rates. For the isotropic 2.1 mm Al shielding, the difference between the HEP and CHARM predicted rates is more than a factor of two. The HEP predicted rate is off by a factor of five with respect to the flight rate, whereas that from CHARM by a factor of eleven.

There can be several reasons why such a high discrepancy between predictions and actual in-flight measurements was found. As mentioned before, the energy threshold of the Weibull curve for the Cypress SRAM was not identified when testing at UMCG, so it can vary between 10 and 20 MeV. This difference can be very important for the MEO in which CELESTA was flown because the spectral distribution of the trapped protons is very different from that of lower-altitude low-Earth orbits (LEOs). This spectral distribution difference is shown in Fig. 9. The figure reports the trapped proton fluxes transported through 2.1 mm of Aluminum for the MEO in which CELESTA has flown and a circular sun-synchronous orbit with altitude 800 km and inclination of 98°. As it can be seen, the trapped proton fluxes peak around 10–20 MeV for this MEO, whereas they peak at 100 MeV for the LEO. Therefore, varying the energy threshold can have a severe impact on the rate estimation for this SRAM.

A second reason to point out is that an isotropic aluminum shielding of just 2.1 mm of thickness was considered. However, the protons coming from the backside of the payload have to transverse far more material. The effect of variable shielding can have significant consequences on error rate estimations for space applications [37]. On average, it was estimated that this material can be 20 mm thick for the backside hemisphere. Fig. 9 shows what happens when the trapped proton fluxes of this MEO are transported through this larger amount of material. The obtained fluxes tend to assume a shape that is far more similar to that of the considered LEO with proton fluxes peaking just below 100 MeV. In this case, since the spotlight is on the environmental fluxes, this hypothesis affects not only the Cypress SRAM estimations but also those for the Brilliance SRAM although to a lesser extent due to the lower sensitivity to lower energy protons.

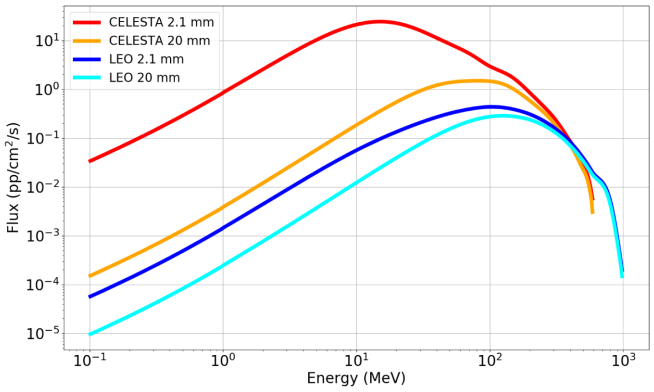

Fig. 9. Comparison of spectral distributions of trapped proton fluxes for the MEO in which CELESTA was flown and a more standard LEO. Both are calculated with the same 2.1 mm spherical aluminum shielding. Trapped proton fluxes transported through 20 mm of aluminum are also shown for the MEO in which CELESTA was flown and the LEO. Data from CREME [38].

The effect of the variable shielding is evaluated first to check what happens to the predicted rates for both the Cypress and Brilliance SRAMs. One-half of the space fluxes, those coming from the 2π sr solid angle on top of the SRAMs, are transported through 2.1 mm of Aluminum, whereas the other half, for those protons passing through the rest of the CubeSat volume, are transported through 20 mm of aluminum.

The effect of the additional shielding on the backside has reduced the expected SEL rate for the Brilliance SRAM as shown in Table III. This reduction is quantified on the order of 30% for the HEP case and 39% for the CHARM case. As shown in the table, these new predicted rates are even closer to the actual flight measurements than with the isotropic 2.1 mm aluminum shielding.

Concerning the Cypress SRAM, the upset rate estimations are reported in Table IV. The discrepancy reaches almost 43% for both HEP and CHARM cases, so the error in the estimation has been cut by almost half. There remains, nonetheless, a factor of three difference between PSI-based predictions and estimations and about six for CHARM.

For the Cypress SRAM, the previous calculation can be repeated, this time considering the energy threshold for the Weibull curve to be 20 MeV. This same energy was already used for the calculations based on the CHARM cross section, so no change in estimation can be expected for this case.

The data for this additional calculation are given in Table IV. Note that the change in energy threshold for the proton cross section resulted in an additional reduction so that HEP-based predictions are now off by just a factor of two with respect to the flight rate.

Different calculation methods are also introduced to verify if the calculation method can have an impact on the predicted rate. Instead of a Weibull curve one can, for instance, employ a Bendel fitting curve. The Bendel fit proposed here for the Cypress SRAM was obtained from OMERE by inputting the data points in Fig. 8 and using the fitting function available in OMERE. The resulting fitting parameters are given in the caption of Table IV. As shown, the Bendel fitting provides results which fall in between those of the two Weibull fits with different energy thresholds.

Finally, the figure of merit (FOM) method has also been tried for the proton rate estimation. Based on [36], the rate for protons can be calculated for this orbit based on the saturation cross section by multiplication with a fixed FOM slope (4.5×10^4) and by an orbit flux-dependent coefficient. The latter, for the 2.1 mm isotropic Al shielding is 600 and for the mixed shielding is 360. The results are reported in Table IV. The FOM returns predicted rates which are very close to the actual in-flight rate and, as such, can be considered the most accurate.

Another reason to justify some of the discrepancies observed is connected to the experimental data collection performed at ground facilities. It is known that the Cypress SRAM may experience some complex behaviors while exposed to high energy beams at high fluxes that can result in a burst of errors recorded upon a readout [24]. The data which were collected at UMCG did not make use of any error burst correction. It was seen before that these issues may cause an overestimation of the SEU cross section measured during an accelerated test of up to a factor of two for this SRAM for cyclotron experiments. A similar situation may happen in CHARM where the beam is delivered in short pulses (300 ms). On the other hand, these bursts are very unlikely to occur when the proton flux is as low as that in space. In fact, these bursts are typically a few hundred errors per readout, and such a significant jump in the cumulative SEU readout was not observed for the in-flight data.

It can be concluded that good accuracy in the predictions was obtained for the SEL in-flight measurements with respect to both estimations coming from high-energy proton and mixed-field testing. Some larger discrepancies were observed for the SEU data which can be due to the inaccurate determination of the energy threshold and high sensitivity with respect to this parameter in this MEO as well as to possible bursts of errors providing a SEU cross section overestimation in ground facilities. Nevertheless, the FOM method also returns compatible expectations for the Cypress SRAM.

V. Conclusion

The CELESTA CubeSat brought to space CERN radiation dosimetry technology based on RADFET for TID measurements and SRAMs for SEU and SEL measurements which can be correlated to the proton/ion fluxes. The final orbit was a MEO, and the mission duration was roughly two months. During this period, the radiation monitoring payload on-board performed measurements of the radiation environment in this orbit. This article has documented the SEE data recorded on-board the CubeSat.

This article reports a comparison of the measured in-flight data rates for SEL and SEU against rates predicted through the expected environment models available in the OMERE tool suite. The peculiar trapped proton spectral distribution of the MEO in which the CubeSat has flown can lead to stronger overestimations of the response if a parameter like the actual shielding configuration of the satellite is not taken into account. In a similar vein, if the proton energy threshold determination is overlooked during the testing activity at

ground facilities, this can introduce a large uncertainty when it comes to predicting the space rate.

Finally, this article showed that fewer discrepancies are to be expected for SEL predictions when using the mixed-field HEH_{eq} cross section as opposed to the high-energy proton Weibull curve than it would be for SEUs. In general, the CHARM mixed-field allows similar SEU predictions than with using protons. What is shown here is that this may be more or less the case when the spectral distribution of protons in space is different at low energies than that available at CHARM.

REFERENCES

[1] H. D. R. Evans, P. Bühler, W. Hajdas, E. J. Daly, P. Nieminen, and A. Mohammadzadeh, "Results from the ESA SREM monitors and comparison with existing radiation belt models," *Adv. Space Res.*, vol. 42, no. 9, pp. 1527–1537, Nov. 2008.

[2] M. Ruffenach, S. Bourdarie, J. Mekki, D. Falguère, and J. R. Vaillé, "Proton radiation belt anisotropy as seen by ICARE-NG Head-A," *IEEE Trans. Nucl. Sci.*, vol. 66, no. 7, pp. 1753–1760, Jul. 2019.

[3] R. Harboe-Sorensen et al., "From the reference SEU monitor to the technology demonstration module on-board PROBA-II," *IEEE Trans. Nucl. Sci.*, vol. 55, no. 6, pp. 3082–3087, Dec. 2008.

[4] R. Harboe-Sorensen et al., "The technology demonstration module on-board PROBA-II," *IEEE Trans. Nucl. Sci.*, vol. 58, no. 3, pp. 1001–1007, Jun. 2011.

[5] F. Bezerra, R. Ecoffet, E. Lorfevre, A. Samaras, and C. Deneau, "CARMEN2/MEX: An in-flight laboratory for the observation of radiation effects on electronic devices," in *Proc. 12th Eur. Conf. Radiat. Effects Compon. Syst.*, Seville, Spain, Sep. 2011, pp. 607–614.

[6] A. Samaras, F. Bezerra, E. Lorfevre, and R. Ecoffet, "CARMEN-2: In flight observation of non destructive single event phenomena on memories," in *Proc. 12th Eur. Conf. Radiat. Effects Compon. Syst.*, Seville, Spain, Sep. 2011, pp. 839–848.

[7] A. L. Bogorad, J. J. Likar, R. E. Lombardi, S. E. Stone, and R. Herschitz, "On-orbit error rates of RHBD SRAMs: Comparison of calculation techniques and space environmental models with observed performance," *IEEE Trans. Nucl. Sci.*, vol. 58, no. 6, pp. 2804–2806, Dec. 2011.

[8] R. Harboe-Sorensen et al., "PROBA-II technology demonstration module in-flight data analysis," *IEEE Trans. Nucl. Sci.*, vol. 59, no. 4, pp. 1086–1091, Aug. 2012.

[9] M. D'Alessio et al., "SRAMs SEL and SEU in-flight data from PROBA-II spacecraft," in *Proc. 14th Eur. Conf. Radiat. Effects Compon. Syst. (RADECS)*, Oxford, U.K., Sep. 2013, pp. 1–8.

[10] B. D. Sierawski et al., "CubeSats and crowd-sourced monitoring for single event effects hardness assurance," *IEEE Trans. Nucl. Sci.*, vol. 64, no. 1, pp. 293–300, Jan. 2017.

[11] D. Alexander et al., "Single event upset results from the radiation hardened electronic memory experiment on the international space station," in *Proc. IEEE Radiat. Effects Data Workshop Rec.*, Waikoloa, HI, USA, Jul. 2018, pp. 131–135.

[12] D. Alexander et al., "Single event upset results from the radiation hardened electronic memory experiment in a polar orbit," in *Proc. IEEE Radiat. Effects Data Workshop Rec.*, Santa Fe, NM, USA, Jul. 2020, pp. 35–38.

[13] N. Kerboub et al., "Comparison between in-flight SEL measurement and ground estimation using different facilities," *IEEE Trans. Nucl. Sci.*, vol. 66, no. 7, pp. 1541–1547, Jul. 2019.

[14] M. Pinto, P. Gonçalves, J. Sampaio, T. Sousa, and C. Poivey, "CTTB memory test board single event effect geostationary in-flight data analysis," in *Proc. RADECS Conf.*, Vannes, France, Oct. 2020, pp. 165–170.

[15] J. J. Likar, C. H. Pham, D. Wilson, A. Coburger, J. Atchison, and J. Porter, "Initial in-flight error rates for 16-MB SRAM as flying on the double asteroid redirection test (DART) mission," *IEEE Trans. Nucl. Sci.*, vol. 70, no. 4, pp. 426–433, Apr. 2023.

[16] F. Bezerra et al., "14 years of in-flight experimental data on CARMEN-MEX," *IEEE Trans. Nucl. Sci.*, vol. 70, no. 8, pp. 1533–1540, Aug. 2023.

[17] D. Alexander et al., "Single event upset results from the radiation hardened electronic memory experiment in a geostationary orbit," in *Proc. IEEE Radiat. Effects Data Workshop Rec.*, Kansas City, MO, USA, Jul. 2023, pp. 230–233.

[18] E. L. Petersen, J. C. Pickel, J. H. Adams, and E. C. Smith, "Rate prediction for single event effects—A critique," *IEEE Trans. Nucl. Sci.*, vol. 39, no. 6, pp. 1577–1599, Dec. 1992.

[19] E. L. Petersen, V. Pouget, L. W. Massengill, S. P. Buchner, and D. McMorrow, "Rate predictions for single-event effects—Critique II," *IEEE Trans. Nucl. Sci.*, vol. 52, no. 6, pp. 2158–2167, Dec. 2005.

[20] R. A. Reed et al., "Single-event effects ground testing and on-orbit rate prediction methods: The past, present, and future," *IEEE Trans. Nucl. Sci.*, vol. 50, no. 3, pp. 622–634, Jun. 2003.

[21] M. Pinto et al., "Parametric evaluation of the SEE rate on the SEU and SEL monitors aboard the Alphasat using the IRPP model," *IEEE Trans. Nucl. Sci.*, vol. 70, no. 8, pp. 1821–1828, Aug. 2023.

[22] G. Spiezia et al., "A new RadMon version for the LHC and its injection lines," *IEEE Trans. Nucl. Sci.*, vol. 61, no. 6, pp. 3424–3431, Dec. 2014.

[23] R. Secondo, "Upgrades of the RadMon V6 and its integration on a nanosatellite for the analysis and the comparative study of the CHARM and low Earth orbit environments," Ph.D. thesis, Institute d'Électronique et des Systèmes, Université de Montpellier, Montpellier, France, 2017.

[24] R. Secondo et al., "Embedded detection and correction of SEU bursts in SRAM memories used as radiation detectors," *IEEE Trans. Nucl. Sci.*, vol. 63, no. 4, pp. 2168–2175, Aug. 2016.

[25] R. Secondo et al., "Analysis of SEL on commercial SRAM memories and mixed-field characterization of a latchup detection circuit for LEO space applications," *IEEE Trans. Nucl. Sci.*, vol. 64, no. 8, pp. 2107–2114, Aug. 2017.

[26] R. Secondo et al., "System level radiation characterization of a 1U CubeSat based on CERN radiation monitoring technology," *IEEE Trans. Nucl. Sci.*, vol. 65, no. 8, pp. 1694–1699, Aug. 2018.

[27] J. Mekki et al., "CHARM: A mixed field facility at CERN for radiation tests in ground, atmospheric, space and accelerator representative environments," *IEEE Trans. Nucl. Sci.*, vol. 63, no. 4, pp. 2106–2114, Aug. 2016.

[28] A. Coronetti et al., "SEU characterization of commercial and custom-designed SRAMs based on 90-nm technology and below," in *Proc. IEEE Radiat. Effects Data Workshop Rec.*, Santa Fe, NM, USA, Dec. 2020, pp. 56–63.

[29] R. G. Alía, S. Uznanski, S. Danzeca, V. Ferlet-Cavrois, and M. Muschitiello, "ESA/CERN heavy ion test campaign at UCL-March 2015," CERN EDMS, Geneva, Switzerland, Tech. Rep., 1533432, v. 1, Sep. 2015.

[30] K. Roed et al., "Method for measuring mixed field radiation levels relevant for SEEs at the LHC," *IEEE Trans. Nucl. Sci.*, vol. 59, no. 4, pp. 1040–1047, Aug. 2012.

[31] *TRAD OMERE (Outil De Modélisation De L'Environnement Radiatif Externe)*. Accessed: Apr. 2022. [Online]. Available: trad.fr/spatial/logiciel-omere/

[32] D. M. Sawyer and J. I. Vette, "AP-8 trapped proton environment for solar maximum and solar minimum," NASA/Goddard Space Flight Center, Greenbelt, MD, USA, Tech. Rep., NSSDC/WDC-A-R&S 76, Dec. 1976.

[33] *Space Environment (Natural and Artificial)—Galactic Cosmic Ray Model*, Standard ISO GCR 15390, ISO TC20/SC14, Jun. 2004.

[34] R. G. Alía et al., "Energy dependence of tungsten-dominated SEL cross sections," *IEEE Trans. Nucl. Sci.*, vol. 61, no. 5, pp. 2718–2726, Oct. 2014.

[35] W. J. Stapor, J. P. Meyers, J. B. Langworthy, and E. L. Petersen, "Two parameter Bendel model calculations for predicting proton induced upset (ICs)," *IEEE Trans. Nucl. Sci.*, vol. 37, no. 6, pp. 1966–1973, Dec. 1990.

[36] E. L. Petersen, "The SEU figure of merit and proton upset rate calculations," *IEEE Trans. Nucl. Sci.*, vol. 45, no. 6, pp. 2550–2562, Dec. 1998.

[37] A. Varotsou et al., "Shielding geometry effect on SEE prediction using the new OMERE release: JASON-2 mission case study," in *Proc. 12th Eur. Conf. Radiat. Effects Compon. Syst.*, Seville, Spain, Sep. 2011, pp. 849–853.

[38] (2023). *CREME*. Vanderbilt University. Accessed: Aug. 2023. [Online]. Available: https://creme.isde.vanderbilt.edu